Article

# REDOX POTENTIAL STUDIES BASED ON SCAN-RATE ANALYSIS OF THE DIFFUSIONAL CONTROL AND DFT CALCULATIONS OF THE SCHIFF BASE [(*E*)-4-AMINO-3-((3,5-DI-*tert*-BUTYL-2-HYDROXYBENZYLIDENE)AMINO) BENZOIC ACID]

**Rosaly Morales-Guevara[a,b], Dayán Páez-Hernández[a], Manuel Gacitúa[c,d,e,*], Juan A. Fuentes[f] and Alexander Carreño[a,g,*]**

[a]Laboratorio de Síntesis Organometálica, Centro de Nanociencias Aplicadas (CANS), Facultad de Ciencias Exactas, Universidad Andres Bello, República 330, 8370186 Santiago, Chile

[b]Departamento de Química de los Materiales, Facultad de Química y Biología, Universidad de Santiago de Chile, Av. Libertador B. O'Higgins 3363, 9170022 Santiago, Chile

[c]Facultad de Ingeniería y Ciencias, Universidad Diego Portales, Ejercito 441, 8370191 Santiago, Chile

[d]Center for the Development of Nanoscience and Nanotechnology, CEDENNA, Avenida Alameda Libertador Bernardo O'Higgins 3363, 9170124 Santiago, Chile

[e]Centro de Nanociencia, Nanotecnología y Desarrollos Avanzados, Ejercito 441, 8370191 Santiago, Chile

[f]Laboratorio de Genética y Patogénesis Bacteriana, Facultad de Ciencias de la Vida, Universidad Andres Bello, República 330, 8370186 Santiago, Chile

[g]Fondecyt Regular 1230917, Agencia Nacional de Investigación y Desarrollo (ANID), Ministerio de Ciencia, Tecnología, Conocimiento e Innovación, Gobierno de Chile, 8370186 Santiago, Chile

Received: 11/02/2023; accepted: 02/23/2024; published online: 04/29/2024

Schiff bases are diverse organic compounds with an azomethine structure (–C=N–), holding potential in both chemistry and biology. They serve as catalysts, stabilizers, and exhibit various biological activities. The molecular structure of Schiff bases influences their biological properties, including antimicrobial effects. Redox-active compounds with more negative potentials tend to be more effective against microbes. In one of our recent studies, we explored the antimicrobial properties of two Schiff bases derivatives, **SB-1** ((*E*)-4-amino-3-((3,5-di-*tert*-butyl-2-hydroxybenzylidene)amino) and **SB-2** ((*E*)-2-((4-nitrobenzilidene)amino)aniline). **SB-1** showed antibacterial activity against certain Gram-positive bacteria, while **SB-2** did not. The difference in their cyclic voltametric profiles, especially **SB-1**'s more negative reduction potential, prompted us to carry out further characterizations, including scan-rate studies, solvent analysis, and computational calculations. We found that **SB-1**, which presents a stable intramolecular hydrogen bond, undergoes irreversible oxidation, likely at the $–NH_2$ group, and a *quasi*-reversible reduction *via* an intramolecular reductive coupling of the (–C=N–) azomethine group, supported by orbital theoretical calculations. This research sheds light on the potential applications of Schiff bases in antimicrobial contexts, guided by their redox properties and structure.

Keywords: Schiff bases; intramolecular hydrogen bond; scan-rate studies; DFT; electron density.

## INTRODUCTION

Schiff bases are a diverse group of organic compounds characterized by an azomethine structure (–C=N–), featuring a double bond linking carbon and nitrogen atoms.[1-3] Numerous Schiff bases have been synthesized, incorporating many combinations of alkyl or aryl substituents,[4,5] thereby inspiring extensive research in the fields of chemistry and biology.[6-10] Schiff bases display a wide range of chemical applications, such as their utilization as catalysts, stabilizers, and intermediates in organic synthesis.[11-14] Moreover, they exhibit significant biological potential, manifesting antiproliferative, anti-inflammatory, antiviral, antimalarial, antifungal, antibacterial, and antipyretic activities.[15-20] It has been reported[21-24] that the molecular structure of Schiff bases can influence biological activities, including antimicrobial properties. Additionally, the structure determines other properties, such as affinity for various targets in biological systems, stability in biological media, and cellular uptake. These factors plausibly contribute to the observed biological activities, particularly the antimicrobial capacity. Therefore, conducting studies to enhance the characterization of these Schiff bases can significantly contribute to a well understanding of the molecular mechanisms underlying these biological activities.

Redox-active of natural compounds or their structural derivatives have the ability to inhibit pathogen growth by disrupting cellular redox homeostasis or the function of redox-sensitive cellular components. This disruption of redox balance has been associated with antimicrobial activity, suggesting a correlation between the redox potential and antimicrobial effectiveness.[25,26] In this sense, the electrochemistry has been gaining attention as a tool to characterize compounds exhibiting antimicrobial properties and other biological activities.[27] In our recent study,[24] we investigated the antimicrobial activity of two Schiff bases derivatives, **SB-1** [(*E*)-4-amino-3-((3,5-di-*tert*-butyl-2-hydroxybenzylidene)amino) benzoic acid], see Scheme 1, and **SB-2** [(*E*)-2-((4-nitrobenzilidene)amino)aniline], against Gram-positive bacteria. **SB-1** demonstrated antibacterial

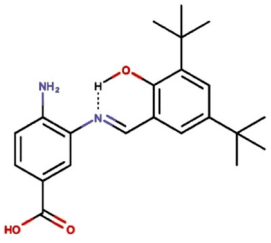


***Scheme 1.*** *Chemical structure of [(E)-4-amino-3-((3,5-di-tert-butyl-2-hydroxybenzylidene)amino) benzoic acid] benzoic acid (**SB-1**)*

*e-mail: alexander.carreno@unab.cl; manuelgacitua@gmail.com

effects against *Staphylococcus aureus*, *Enterococcus faecalis*, and *Bacillus cereus*, similar to chloramphenicol, while **SB-2** exhibited no effect on these bacteria. Given the observed differences in the cyclic voltametric profiles of these two Schiff bases, with **SB-1** displaying a more negative reduction potential (**SB-1** $Red^{I}_{(irr)}$: –0.90 V; **SB-2** $Red^{II}_{(rev)}$: –0.80 V) and a more positive oxidation potential compared to **SB-2** (**SB-1** $Ox^{I}_{(irr)}$: 1.23 V; **SB-2** $Ox^{I}_{(irr)}$: 0.94 V), we conducted a complementary characterization of **SB-1**. This included a scan-rate study to determine whether these processes are diffusion-controlled. Additionally, we employed previously untested deuterated solvents with varying polarities (chloroform, acetonitrile, and acetone) for further characterization of the **SB-1** structure. Fourier transform infrared-attenuated total reflectance (ATR-FTIR) and ultraviolet visible spectrophotometry (UV-Vis) techniques were also utilized. Furthermore, quantum chemistry calculations were performed to corroborate the redox potentials and generate electron density maps, clarifying the regions where reductions or oxidations occur in the carbon backbone.

## Quantum chemistry theory

All the work presented in this study was conducted within the relativistic density functional theory framework using the Amsterdam density functional (ADF) code.[28] The molecular structures were fully optimized using the hybrid B3LYP functional,[29,30] and the standard Slater-type orbital (STO) basis set with triple-ζ quality and double plus polarization functions (TZ2P) for all atoms.[31,32] Frequency analysis was performed to obtain thermodynamic parameters used to determine the redox potentials. Additionally, solvation energies were estimated using a conductor-like screening model (COSMO),[33,34] with the parameters specific to acetonitrile. The second part of the calculations aimed to determine the equilibrium oxidation and reduction potentials.[35,36] To establish the computational protocol for estimating the redox potentials, reference to the thermodynamic cycle,[37-41] depicted in Figures 1 and 2 proved to be valuable. The standard Gibbs free energies (in acetonitrile) were obtained by performing calculations in both gas phase and solution for the reduced and oxidized species. The gas phase free energies were derived from single-point energy calculations, followed by frequency calculations employing Equation 1:

$$\Delta G_s^0(\text{redox, acetonitrile}) = \Delta G_s^0(\text{redox, gas}) + \Delta G_s^0(\text{FO}) - \Delta G_s^0(\text{FR}) \quad (1)$$

The standard absolute redox potential ($E^0$) can be calculated using the Equation 2:

$$E^0 = -\Delta G_s^0(\text{redox, acetonitrile})/\,nF \quad (2)$$

In the given Equation 2, n represents the number of electrons consumed or generated in the specific half-reaction, and F denotes the Faraday constant. This thermodinamic model establishes a direct connection between the changes in free energy in the condensed phase related to reduction or oxidation and the corresponding processes in the gas phase. Furthermore, in order to determine the free energy associated with ionization or electron attachment at 298 K, it is essential to calculate the thermal contributions to the free energy at 298 K.

Taking this into consideration, the remaining link between the gas and the condensed phase is defined by the difference in solvation free energies between the species oxidized and reduced involved in the respective processes. The calculated absolute free energy of reduction or oxidation represents the generation or consumption of a free electron. However, in practical terms, free electrons do not directly participate in reactions. Instead, they are consumed or generated by another half-reaction, respectively.

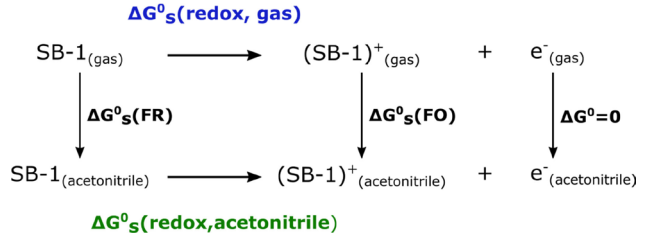


***Figure 1.*** *Thermodynamic free energy cycle employed to calculate the redox potential of the* ***(SB-1)/(SB-1)*****$^{+1}$** *pair. $\Delta G^0_s$ (redox, gas) and $\Delta G^0_s$ (redox, acetonitrile) represent the free energy change for the redox process in the gas phase and in the presence of acetonitrile, respectively. Furthermore, $\Delta G^0_s$ (FR) and $\Delta G^0_s$ (FO) denote the solvation free energy change for the reduced and oxidized forms*

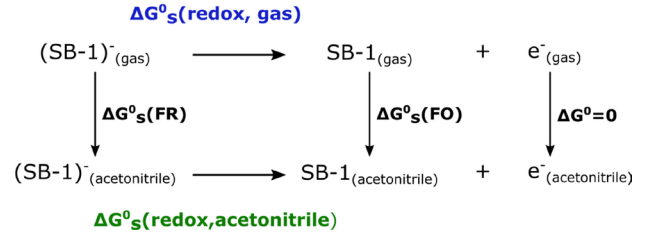


***Figure 2.*** *Thermodynamic free energy cycle employed to calculate the redox potential for* ***(SB-1)*****$^{-1}$****/(SB-1)** *pair. $\Delta G^0_s$ (redox, gas) and $\Delta G^0_s$ (redox, acetonitrile) represent the free energy change for the redox process in the gas phase, and in the presence of acetonitrile, respectively. Additionally, $\Delta G^0_s$ (FR) and $\Delta G^0_s$ (FO) denote the solvation free energy change for the reduced and oxidized form*

## EXPERIMENTAL

The Fourier transform infrared-attenuated total reflectance (ATR-FTIR) spectra were acquired using a FT-IR Spectrometer Spectrum Two (PerkinElmer, Chile). The $^1$H NMR and $^{13}$C NMR spectra of **SB-1** were recorded on a Bruker AVANCE III HD-400 (FONDEQUIP EQM120021, Unidad Central de Instrumentación, Facultad de Química y de Farmacia, Pontificia Universidad Católica de Chile, Chile) operating at 400 MHz and maintained at 25 °C. All samples were dissolved in deuterated chloroform, acetone, or acetonitrile, with tetramethylsilane serving as the internal reference. Values of $\delta$ in ppm and $J$ in Hz. For the electrochemical experiments, see Supplementary Material.[42,43]

### Materials

The reagents employed in the synthesis were commercially available from Aldrich (Aldrich, Chile) and were used as received without additional purification.

### Chemical

The (*E*)-4-amino-3-((3,5-di-*tert*-butyl-2-hydroxybenzylidene) amino)benzoic acid (**SB-1**) was prepared by direct condensation of primary amine with their corresponding substituent benzaldehyde, according to a previously described method (see Scheme 1S).[6,8,24] Further information can be found in the Supplemetary Material.

## RESULTS AND DISCUSSION

### Synthesis and characterizations of SB-1

The (*E*)-4-amino-3-((3,5-di-*tert*-butyl-2-hydroxybenzylidene) amino) benzoic acid (referred to as **SB-1**) was synthesized through the direct condensation of amino benzoic acid and the corresponding phenol aldehyde (Scheme 1S in the Supplementary Material). Previously, we reported the structure of **SB-1**, which was determined using NMR analysis in deuterated dimethyl sulfoxide (DMSO). The analysis revealed the presence of an intramolecular hydrogen bond (IHB) between the N atom of the Schiff base and the –OH group of the phenolic ring, providing stability.[24] The significance of the IHB has been demonstrated in similar Schiff bases, influencing both their photophysical properties and biological activities.[6,8,41,44,45] In light of this, our aim was to further characterize the stability of the IHB in **SB-1** by examining its behavior in previously untested deuterated solvents with varying dielectric constants, namely chloroform ($\varepsilon = 4.81$), acetone ($\varepsilon = 20.7$), and acetonitrile ($\varepsilon = 37.5$). We sought to determine whether solvent polarity could influence the IHB. To achieve this, we conducted $^{1}H$ and $^{13}C$ NMR analyses at 25 °C. Notably, the key signals corresponding to the –OH and $–NH_2$ groups, as well as the protons of the azomethine moiety, consistently appeared at approximately 13.30, 5.79, and 8.84 ppm, respectively, across all solvents (see Figures 1S to 4S in the Supplementary Material). Table 1 provides the principal proton assignments. In less stable IHBs, interactions with polar solvents like acetone or acetonitrile typically result in destabilization due to intermolecular interactions. Consequently, a shift in the assigned signal positions in the $^{1}H$ NMR spectrum is expected. Conversely, no changes are anticipated in more stable IHBs, regardless of the solvent used. This approach has been previously employed to assess IHB stability in other pyridine Schiff bases.[41,46] Confirming the stability of the IHB, its peak remained consistently at the same position (approximately 13.30 ppm) in all the solvents tested, regardless of their dielectric constants. Furthermore, the proton associated with the azomethine group (–CH=N–), H4, exhibited a singlet peak at approximately 8.96-8.68 ppm.

**Table 1.** Summary of the most important protons of **SB-1** compound found with the $^{1}H$ NMR

| Deuterated solvents | –OH / ppm | $–NH_2$ / ppm | Azomethine proton (H4) / ppm | –COOH / ppm |
|---|---|---|---|---|
| DMSO[a] | 13.36 | 5.79 | 8.93 | 12.24 |
| Chloroform | 13.06 | 6.72 | 8.68 | 11.58 |
| Acetone | 13.44 | 5.50 | 8.96 | Not observed |
| Acetonitrile | 13.34 | 4.98 | 8.82 | Not observed |

[a] $^{1}H$ NMR (400 MHz).[24] DMSO: dimethyl sulfoxide.

The signals assigned to the *tert*-butyl groups appear at 1.47 and 1.28 ppm. The aromatic protons of aromatic rings appear at 7.50-6.70 and 8.60-8.00 ppm, respectively. The $^{13}C$ NMR was recorded in deuterated chloroform and acetonitrile, showing the azomethine carbon around 170 ppm in agreement with similar Schiff bases(see Figures 5S and 6S in the Supplementary Material).[8,47]

On the other hand, the absorption spectra of **SB-1** were studied in three organic solvents of increasing polarity (chloroform, acetonitrile, and DMSO) at room temperature. In the presence of chloroform, acetonitrile, or DMSO, we observed that **SB-1** presented two intense absorption bands around 281 and 377 nm (Table 2 and Figure 7S in the Supplementary Material). The band around 281 nm corresponds to the $\pi \rightarrow \pi^*$ of the aromatic rings, by analogy with similar Schiff bases compounds.[6,48,49] The band around 377 nm was assigned to a combination of $\pi \rightarrow \pi^*$ and $n \rightarrow \pi^*$ ligand transitions (which involves the IHB). In the case of **SB-1**, we observed no significant shifts in the IHB band, independent of the solvent used.

**Table 2.** Summarized absorption properties in DMSO, chloroform, and acetonitrile for **SB-1**

| Schiff bases | Solvent | $\lambda_{max}$ / nm | $\xi$ / (dm$^3$ mol$^{-1}$ cm$^{-1}$) |
|---|---|---|---|
| **SB-1** | DMSO | 283 | 30571 |
| | | 385 | 10737 |
| | acetonitrile | 280 | 34765 |
| | | 373 | 12084 |
| | chloroform | 282 | 33216 |
| | | 373 | 12339 |

$\lambda_{max}$: Wavelength at which a substance has its strongest photon absorption; $\xi$: molar extinction coefficient; DMSO: dimethyl sulfoxide.

**SB-1** exhibits no luminescent properties plausibly due to the rigidity of the structure, which substantially reduces the vibronic relaxation.[50,51] This agrees with the change in the molecule's configuration when excitation occurs in similar systems containing the azomethine group.[41] The ATR-FTIR spectrum was used to confirm the **SB-1** structure. Two bands at 3475 and 3379 cm$^{-1}$ were assigned to the stretching vibrations mode (asymmetric and symmetric mode) of νNH (primary amino group) (Figure 8S in the Supplementary Material). These assignments are congruent with previously reported studies.[6,8,52] It is important to remark that, due to the ATR-FTIR limitations,[53] the bands assigned to the –OH appeared to be thinner than the bands obtained with the KBr pellet. Other authors[54] reported broader bands in the 3500-3000 cm$^{-1}$ range due to the stretching νOH group engaged in the IHB. Nevertheless, we could not observe those bands in our ATR-FTIR spectrum, probably due to the overlapping with the bands assigned to νNH. We also assigned other bands observed at 2960 and 2867 cm$^{-1}$ as νOH or νC–OH and νC–H, respectively. Other remarkable bands were observed at 1608 and 1559 cm$^{-1}$, assigned as νHC=N (azomethine) and νC=C, respectively. It is worth underlining that the azomethine group is usually assigned to around 1640 cm$^{-1}$. The lower values observed for νHC=N can be explained by the interaction of the azomethine and the hydroxyl groups, both involved in the IHB, as previously reported for similar Schiff bases.[6,8,41] These results: $^{1}H$ NMR, $^{13}C$ NMR, UV-Vis, and ATR-FTIR together corroborate the high stability of IHB and, more importantly, the purity of the **SB-1** powder that was subsequently used for electrochemical tests.

### Scan-rate study

The cyclic voltammetry for **SB-1** was already performed in anhydrous $CH_3CN$ under an argon atmosphere. Several oxidation and reduction processes were identified by direct analysis of the cyclic voltammograms.[24] In this work, we conducted a complementary characterization of **SB-1** using a scan-rate study to determine whether these processes are diffusion-controlled. For **SB-1**, a scan-rate study was performed (Figure 3), where one oxidation at 1.23 V (irreversible) and one reduction at –0.90 V (*quasi*-reversible) were observed. Table 3 summarizes the description of signals, and Table 4 shows the scan-rate study.

**SB-1** profile presents at least one irreversible oxidation process, as previously described for similar Schiff bases with an intramolecular hydrogen bond.[41,46] The nature of this irreversible oxidation is typically ascribed to an oxidation taking place somewhere at the aminobenzoic ring, most likely at the $–NH_2$ moiety.[6] On the other hand, the

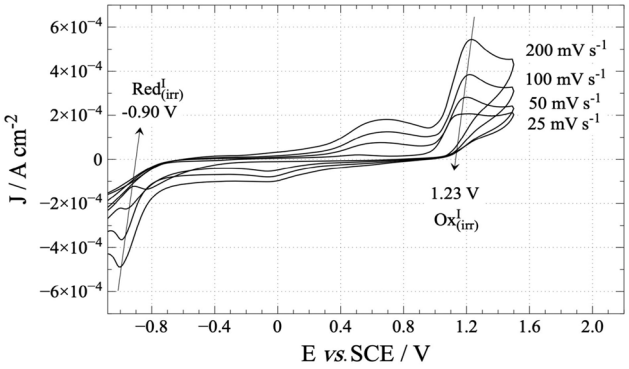


***Figure 3.*** *Scan-rate study for* ***SB-1****. Interphase: Pt|1.0 × 10⁻² M of compound + 1.0 × 10⁻¹ M TBAPF₆ in anhydrous CH₃CN*

*quasi*-reversible reduction may be attributed to an intramolecular reductive coupling of the azomethine group, which involved a self-protonation reaction.[55,56] As discussed below, molecular models and the frontier orbitals HOMO-LUMO were carried out to complement these assignations.

## Quantum chemical results

In order to better understand the nature of the redox processes described above, we performed theoretical calculations using the thermodynamic cycle. We found 1.67 and –0.90 V for the oxidation and reduction process, respectively, of **SB-1**, reproducing the same experimental trend (Table 3). On the other hand, we calculated the probability of finding an electron at a specific location around the aromatic rings or the azomethine group using electron density plots (Figure 4).

We observed that HOMO is mainly distributed in the benzoic acid ring, where oxidation is most likely to occur. Besides, the considerable potential difference in oxidation peaks obtained with calculations could be explained by the electron withdrawal influence of the carboxylic acid group on **SB-1**, which increases the energy (potential) required to oxidize the amine group. In the case of LUMO, it is predominantly distributed between the two aromatic rings, showing a preference for the azomethine group. As stated above, the reduction processes in this kind of compound are found in the azomethine group,[41,57] which is presumably related to the reduction of the N–H bond distance (H of the intramolecular hydrogen bond) found in the reduced form in the molecule in the calculations.

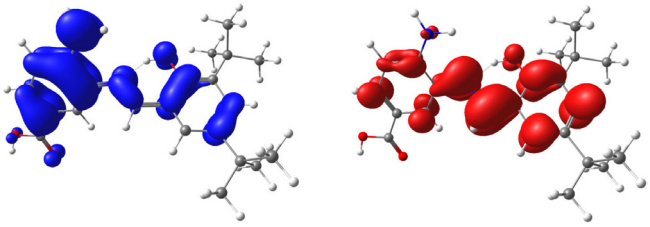

***Figure 4.*** *Electron density for* ***SB-1****: HOMO (blue) and LUMO (red)*

To complement this analysis, an electron density difference map was performed, showing electrons' different occupied regions in the **SB-1** skeleton (Figure 5). The isosurface map between HOMO and LUMO allowed us to better observe the oxidation at the amino group (benzoic acid ring) and the reduction at the azomethine group, corroborating the previous calculations. These results agree with the experimental electrochemical discussion scan-rate study above.

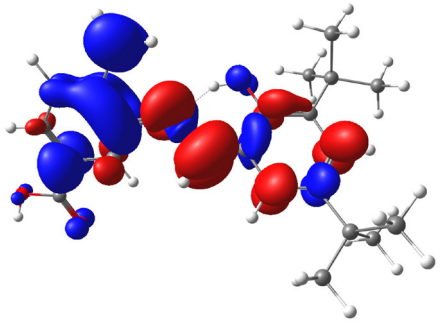

***Figure 5.*** *Electron density difference map between the HOMO and LUMO orbitals for* ***SB-1***

## CONCLUSIONS

In this report, we provided a further characterization of **SB-1** regarding the structure and the redox potential. We found that the intramolecular hydrogen bond in **SB-1** presented a high stability, even in solvents with increased polarity. Furthermore, we determined the electrochemical profile of **SB-1**, providing further details with a scan-rate study. The **SB-1** profile demonstrated an irreversible oxidation process, likely occurring at the pyridine ring's $–NH_2$ group, while its reduction is associated with an intramolecular reductive coupling of the azomethine group, featuring *quasi*-reversibility due to a self-protonation reaction. Molecular models, frontier orbital calculations

**Table 3.** Electrochemical characterization summary of **SB-1**

| **SB-1** | | Potential / V | Reversibility | Diffusion control? |
|---|---|---|---|---|
| Experimental | oxidation$^{I}$ | +1.23 | irreversible | yes |
| | reduction$^{I}$ | –0.90 | *quasi*-reversible | yes |
| Theoretical calculations | oxidation$^{I}$ | +1.67 | – | – |
| | reduction$^{I}$ | –0.90 | – | – |

Potential reported in volts, referenced to an Ag/AgCl electrode in tetramethylammonium chloride to match the potential of a saturated calomel electrode (SCE) at room temperature.

**Table 4.** Scan-rate study results for determining diffusional control of described electrochemical processes at **SB-1**

| Process | Scan-rate *vs* current-density peak | | | (Scan-rate)$^{½}$ *vs* current-density peak | | | Diffusion control? |
|---|---|---|---|---|---|---|---|
| | m | n | $R^2$ | m | n | $R^2$ | |
| $Ox^{I}_{(irr)}$ | $2.0 \times 10^{-6}$ | $1.8 \times 10^{-4}$ | 0.983 | $3.7 \times 10^{-5}$ | $1.6 \times 10^{-5}$ | 0.999 | yes |
| $Red^{I}_{(rev)}$ | $–1.9 \times 10^{-6}$ | $–1.2 \times 10^{-4}$ | 0.943 | $–3.9 \times 10^{-5}$ | $5.0 \times 10^{-5}$ | 0.988 | yes |

m: Slope; n: intercept; $R^2$: linear regression coefficient, (y = mx + n); Ox: oxidation; Red: reduction; irr: irreversible; rev: reversible.

using the thermodynamic cycle and the electron density between HOMO and LUMO were utilized to corroborate these findings.

## SUPPLEMENTARY MATERIAL

Complementary material for this work is available at http://quimicanova.sbq.org.br/, as a PDF file, with free access.

## ACKNOWLEDGMENTS

This work was funded by FONDECYT 1230917 and Núcleo UNAB DI-01-22/NUC. A. Carreño thanks to Núcleo UNAB-DI-02-22/NUC, J. A. Fuentes thanks to FONDECYT 1220584, and R. Morales-Guevara thanks the Ph.D. fellowship ANID 21210811. We thank Juan Manuel Ortega Martínez (Fondecyt Regular 1230917) for his help with the English translation.

## REFERENCES

1. Omidi, S.; Kakanejadifard, A.; *RSC Adv.* **2020**, *10*, 30186. [Crossref]
2. da Silva, C. M.; da Silva, D. L.; Modolo L. V.; Alves, R. B.; de Resende, M. A.; Martins, C. V. B.; de Fátima, A.; *J. Adv. Res.* **2011**, *2*, 1. [Crossref]
3. Carreño, A.; Vega, A.; Zárate, X.; Schott, E.; Gacitúa, M.; Valenzuela, N.; Preite, M.; Manríquez, J. M.; Chávez, I.; *Quim. Nova* **2014**, *37*, 584. [Crossref]
4. Tan, X. J.; Wang, D.; Hei, X. M.; Yang, F. C.; Zhu, Y. L.; Xing, D. X.; Ma, J. P.; *Acta Crystallogr., Sect. C: Struct. Chem.* **2020**, *76*, 44. [Crossref]
5. Sharma, S.; Dubey, G.; Sran, B. S.; Sharma, M.; Kaur, V.; Kaur, S.; Bharatam, P. V.; Hundal, G.; *ChemistrySelect* **2022**, *7*, 1. [Crossref]
6. Carreño, A.; Rodríguez, L.; Páez-Hernández, D.; Martín-Transaco, R.; Zúñiga, C.; Oyarzún, D.; Gacitúa, M.; Schott, E.; Arratia-Pérez, R.; Fuentes, J. A.; *Front. Chem.* **2018**, *6*, 312. [Crossref]
7. Luo, Y.; Wang, J.; Zhang, B.; Guan, Y.; Yang, T.; Li, X.; Xu, L.; Wang, J.; Yo, Z.; *J. Coord. Chem.* **2020**, *73*, 1765. [Crossref]
8. Carreño, A.; Zúñiga, C.; Páez-Hernández, D.; Gacitúa, M.; Polanco, R.; Otero, C.; Arratia-Pérez, R.; Fuentes, J. A.; *New J. Chem.* **2018**, *42*, 8851. [Crossref]
9. Luna, I.; Neves, W. W.; de Lima Neto, R. G.; Albuquerque, A. P. B.; Pitta, M. G. R.; Rêgo, M. J. B. M.; Neves, R. P.; Scotti, M. T.; Mendonça Júnior, F. J. B.; *J. Braz. Chem. Soc.* **2021**, *32*, 1017. [Crossref]
10. Sahu, S. K.; Azam, M. A.; Banerjee, M.; Acharrya, S.; Behera, C. C.; Si, S.; *J. Braz. Chem. Soc.* **2008**, *19*, 963. [Crossref]
11. Jezierska, A.; Tolstoy, P. M.; Panek, J. J.; Filarowski, A.; *Catalysts* **2019**, *9*, 909. [Crossref]
12. Gebrezgiabher, M.; Bayeh, Y.; Gebretsadik, T.; Gebreslassie, G.; Elemo, F.; Thomas, M.; Linert, W.; *Inorganics* **2020**, *8*, 66. [Crossref]
13. Rigamonti, L.; Zardi, P.; Carlino, S.; Demartin, F.; Castellano, C.; Pigani, L.; Ponti, A.; Ferretti, A. M.; Pasin, A.; *Int. J. Mol. Sci.* **2020**, *21*, 7882. [Crossref]
14. Dogaheh, S. G.; Barbero, S.; Barrientos, J.; Janczak, J.; Soleimannejad, J.; Sañudo, E. C.; *Int. J. Mol. Sci.* **2020**, *21*, 3574. [Crossref]
15. Ullah, H.; Rahim, F.; Taha, M.; Hussain, R.; Tabassum, N.; Wadood, A.; Nawaz, M.; Mosaddik, A.; Imran, S.; Wahab, Z.; Abbas Miana, G.; Kanwal; Khan, K. M.; *Arabian J. Chem.* **2020**, *13*, 4904. [Crossref]
16. Prasad, S.; Radhakrishna, V.; Ravi, T. K.; *Arabian J. Chem.* **2019**, *12*, 3943. [Crossref]
17. Venugopala, K. N.; Kandeel, M.; Pillay, M.; Deb, P. K.; Abdallah, H. H.; Mahomoodally, M. F.; Chopra, D.; *Antibiotics* **2020**, *9*, 559. [Crossref]
18. Nastasa, C.; Vodnar, D. C.; Ionut, I.; Stana, A.; Benedec, D.; Tamaian, R.; Oniga, O.; Tiperciuc, B.; *Int. J. Mol. Sci.* **2018**, *19*, 222. [Crossref]
19. Rafiq, K.; Khan, M.; Muhammed, N.; Khan, A.; Rehman, N. U.; Al-Yahyaei, B. E. M.; Khiat, M.; Halim, S. A.; Shah, Z.; Csuk, R.; Al-Harrasi, A.; *Med. Chem. Res.* **2021**, *30*, 712. [Crossref]
20. Aslam, M.; Anis, I.; Mehmood, R.; Iqbal, L.; Iqbal, S.; Khan, I.; Chishti, M. S.; Perveen, S.; *Med. Chem. Res.* **2015**, *25*, 109. [Crossref]
21. Weng, Q.; Yi, J.; Chen, X.; Luo, D.; Wang, Y.; Wang, Y.; Sun, W.; Kang, J.; Han, Z.; *ACS Omega* **2020**, *5*, 24864. [Crossref]
22. Wang, D.; Li, H.; Sun, S.; Xu, Y.; *Org. Lett.* **2020**, *22*, 3361. [Crossref]
23. Reimann, M. J.; Salmon, D. R.; Horton, J. T.; Gier, E. C.; Jefferies, L. R.; *ACS Omega* **2019**, *4*, 2874. [Crossref]
24. Gacitúa, M.; Carreño, A.; Morales-Guevara, R.; Páez-Hernández, D.; Martínez-Araya, J. I.; Araya, E.; Preite, M.; Otero, C.; Rivera-Zaldívar, M. M.; Silva, A.; Fuentes, J. A.; *Int. J. Mol. Sci.* **2022**, *23*, 2553. [Crossref]
25. Kim, J. H.; Cheng, L. W.; Land, K. M.; Gruhlke, M. C. H.; *Front. Microbiol.* **2021**, *12*, 758750. [Crossref]
26. Brzoza, P.; Godlewska, U.; Borek, A.; Morytko, A.; Zegar, A.; Kwiecinska, P.; Zabel, B. A.; Osyczka, A.; Kwitniewski, M.; Cichy, J.; *Antioxidants* **2021**, *10*, 446. [Crossref]
27. Nesmerak, K.; *Mini-Rev. Med. Chem.* **2020**, *20*, 1341. [Crossref]
28. te Velde, G.; Bickelhaupt, F. M.; Baerends, E. J.; Guerra, C. F.; van Gisbergen, S. J. A.; Snijders, J. G.; Ziegler, T.; *J. Comput. Chem.* **2001**, *22*, 931. [Crossref]
29. Raghavachari, K.; *Theor. Chem. Acc.* **2000**, *103*, 361. [Crossref]
30. Al-Busaidi, I. J.; Rashid Ilmi, R.; Dutra, J. D. L.; Oliveira, W. F.; Haque, A.; Al Rasbi, N. K.; Marken, F.; Raithby, P. R.; Khan, M. S.; *Dalton Trans.* **2021**, *50*, 1465. [Crossref]
31. Páez-Hernández, D.; Murillo-López, J. A.; Arratia-Pérez, R.; *Organometallics* **2012**, *31*, 6297. [Crossref]
32. Van Lenthe, E.; Baerends, E. J.; *J. Comput. Chem.* **2003**, *24*, 1142. [Crossref]
33. Klamt, A.; Jonas, V.; Bürger, T.; Lohrenz, J. C. W.; *J. Phys. Chem. A* **1998**, *102*, 5074. [Crossref]
34. Lange, A. W.; Herbert, J. M.; *J. Chem. Phys.* **2011**, *134*, 204110. [Crossref]
35. Jaque, P.; Marenich, A. V.; Cramer, C. J.; Truhlar, D. G.; *J. Phys. Chem. C* **2007**, *111*, 5783. [Crossref]
36. Winget, P.; Weber, E. J.; Cramer, C. J.; Truhlar, D. G.; *Phys. Chem. Chem. Phys.* **2000**, *2*, 1231. [Crossref]
37. Sebens, C. T.; *Foundations of Physics* **2021**, *51*, 75. [Crossref]
38. Psciuk, B. T.; Schlegel, H. B.; *J. Phys. Chem. B* **2013**, *117*, 9518. [Crossref]
39. Sundstrom, E. J.; Xinzheng Yang, X.; Thoi, V. S.; Karunadasa, H. I.; Chang, C. J.; Long, J. R.; Head-Gordon, M.; *J. Am. Chem. Soc.* **2012**, *134*, 5233. [Crossref]
40. Rojas-Poblete, M.; Carreño, A.; Gacitúa, M.; Páez-Hernández, D.; Rabanal-Leóne, W. A.; Arratia-Pérez, R.; *New J. Chem.* **2018**, *42*, 5471. [Crossref]
41. Carreño, A.; Gacitúa, M.; Páez-Hernández, D.; Polanco, R.; Preite, P.; Fuentes, J. A.; Mora, G.; Chávez, I.; Arratia-Pérez, R.; *New J. Chem.* **2015**, *39*, 7822. [Crossref]
42. Diaz, F. R.; Pardo, M. A.; Gacitúa, M. A.; del Valle, M. A.; *J. Chil. Chem. Soc.* **2020**, *65*, 5023. [Crossref]
43. del Valle, M. A.; *Int. J. Electrochem. Sci.* **2019**, *14*, 8131. [Crossref]
44. Morales-Guevara, R.; Fuentes, J. A.; Páez-Hernández, D.; Carreño, A.; *RSC Adv.* **2021**, *11*, 37181. [Crossref]
45. Morales-Guevara, R.; Fuentes, J. A.; Páez-Hernández, D.; Carreño, A.; *J. Phys. Chem. A* **2022**, *126*, 8997. [Crossref]
46. Carreño, A.; Páez-Hernández, D.; Cantero-López, P.; César Zúñiga, C.; Nevermann, J.; Ramírez-Osorio, A.; Gacitúa, M.; Oyarzún, P.; Sáez-Cortez, F.; Rubén Polanco, R.; Otero, C.; Fuentes, J. A.; *Molecules* **2020**, *25*, 2741. [Crossref]
47. Malik, M. A.; Lone, S. A.; Gull, P.; Dar, O. A.; Wani, M. Y.; Ahmad, A.; Hashmi, A. A.; *Med. Chem.* **2019**, *15*, 648. [Crossref]

48. Reddy, K. R.; Raghu, A. V.; Jeong, H. M.; Siddaramaiah; *Des. Monomers Polym.* **2012**, *12*, 109. [Crossref]
49. Zoubi, W. A.; Kandil, F.; *Org. Chem.: Curr. Res.* **2012**, *1*, 1. [Crossref]
50. Gopal, V. R.; Reddy, A. M.; Rao, V. J.; *J. Org. Chem.* **2002**, *60*, 7966. [Crossref]
51. Karatsu, T.; Kitamura, A.; Zeng, H.; Arai, T.; Sakuragi, H.; Tokumaru, K.; *Bull. Chem. Soc. Jpn.* **1995**, *68*, 920. [Crossref]
52. Oketani, R.; Takahashi, H.; Hoquante, M.; Brandel, C.; Cardinael, P.; Coquerel, G.; *J. Mol. Struct.* **2019**, *1184*, 36. [Crossref]
53. Grdadolnik, J.; *Acta Chim. Slov.* **2002**, *49*, 631. [Link] accessed in April 2024
54. Hansen, P. E.; *Molecules* **2021**, *26*, 2409. [Crossref]
55. Venkittapuram, P.; Dhandapani, M.; Suyambulingam, J.; Subramanian, C.; *J. Serb. Chem. Soc.* **2020**, *85*, 215. [Crossref]
56. Zolezzi, S.; Spodine, E.; Decinti, A.; *Polyhedron* **2002**, *21*, 55. [Crossref]
57. Tümer, M.; *J. Coord. Chem.* **2007**, *60*, 2051. [Crossref]